Predicting Land-Cover Changes with Gray Systems Theory and Multitemporal Aerial Photographs

Ruiliang Pu and Peng Gong

Center for Assessment and Monitoring of Forest and Environmental Resources (CAMFER)
Department of Environmental Science, Policy, and Management
151 Hilgard Hall, University of California, Berkeley, CA 94720-3110, USA

Abstract
In this study, we report a new technique based on gray systems theory for land-cover change prediction. Historical land-cover data were obtained from aerial photo interpretation. Change prediction was carried out for seven land-cover types in Claremont Canyon, Alameda County, California. The prediction results demonstrated that the prediction technique was effective.

I. INTRODUCTION

Monitoring and prediction of land-cover/use are critical to the modeling of global change and management of ecosystems. A large number of methods for detecting changes in land surface conditions has been proposed. With remote sensing, a simple but effective method for change detection is taking the difference of the spectral responses at the same spatial location among a set of two or more images acquired at different times (e.g., Kushwaha, 1990; and Franklin and Wilson, 1991). The spectral difference between different times may be extended to differences of multitemporal vegetation indices derived from remotely sensed data (e.g., Hashem et al., 1996). Other techniques include multidate principal component analysis (PCA), Kauth-Thomas transformation of multispectral data (Kauth and Thomas, 1976) and Gramm-Schmidt (GS) orthogonalization (Collins and Woodcock, 1994). Most change detection methods with PCA perform PCA transformation directly to the original multispectral bands acquired at different times, then analyzing several minor principal components to determine change information (location, patterns, and amplitude) (e.g., Collins and Woodcock, 1996, Muchoney and Haack, 1994, and Miller et al., 1998). However, Gong (1993) followed by Parra et al. (1996), employed PCA to difference images which led to better change detection results. Recently, some researchers using artificial neural network (ANN) to predict or detect changes in grass or forest lands (e.g., Tan and Smeins, 1996; Gopal and Woodcock, 1996) thought that a nonlinear technique such as the ANN might be more applicable to describe the change behavior of land use/cover.

In this study, we proposed a new technique to predict changes of land-cover types based on the gray systems theory (GST) (Yuan, 1991) and multitemporal aerial photographs in a relative short time series. A prediction model based on GST is to infer a system condition from the past to the future based on known or indeterminate information of both past and present then to determine the system's tendency of development and change in the future and to provide the basis for planning and decision-making (Yuan, 1991). The GST prediction model may use limited data with a very short time sequence to predict changes of some condition while other techniques such as linear regression and nonlinear neural network algorithms perform improperly or simply do not work under this condition. Therefore, the objective of this study is to demonstrate the effectiveness of the GST model in predicting land-cover changes.

II. STUDY AREA AND AERIAL PHOTOGRAPHS

Study Area

The study area is located at the Claremont Canyon, Alameda County, California. It is a portion of the East Bay Hills of the San Francisco Bay Area, with an area of approximately 250 hectares. The elevation in Claremont Canyon varies from 120 m to 520 m above sea level. The mild climate and relatively large elevation and slope range enable many vegetation types to grow in this area. Primary vegetation types consist of Monterey pine, coastal redwood, and Eucalyptus, cypress, bay/oak woodland, *Baccharis pilularis*, and coyote brush. In addition, the land-cover types have been changing over time due to changes of climate variables and human activities, especially the latter (Sanders and Dow, 1993). Based on the relative stability of existing land-cover types (primary vegetation types) in the Claremont Canyon

and the interpretability of aerial photographs, we defined seven land-cover types (Table 1) for use in this study.

Aerial Photographs

Historical black-and-white aerial photographs covering the Claremont Canyon were used to determine land-cover types. Five sets of black/white aerial photographs were obtained from the library of the University of California at Berkeley for 1947, 1957, 1969, 1979, and 1985. Nominal scales were 1:12,000 for the photos of 1957-1985, 1:20,000 for 1947, and a 1995 digital orthophoto produced from 1: 24,000 aerial photography. The quality of these photos was medium but it is feasible to delineate land-cover types from them based on our knowledge gained in the field.

III. METHODS AND PRINCIPLE

Table 1. Summary of land-cover types

No.	Type	Description
1	MP	Monterey pine stand
2	EU	Eucalyptus with varying density
3	GL	Grass land
4	CP	Cypress stand
5	BA	*Baccharis Pilularis*, Coyote brush
6	BO	Bay laurel and oak woodland
7	RA	Housing, buildings, residential areas

Mapping Land-Cover Types

Land-cover maps were generated by interpreting aerial photographs. The procedure for mapping land-cover types can be divided into five steps as following.

Step 1. Digitize the aerial photos
Multidate analog aerial photos were digitized by scanning them at 300 dpi with a flatbed scanner and saved in TIFF format. Then the TIFF images were read into the PCI image analysis system (PCI, Inc. 1997) for rectification and cover type delineation.

Step 2. Rectify the aerial photos
Because the scales of the multidate aerial photos are not exactly the same and their projection centers varies, it is necessary to rectify them to a common reference. Rectifying aerial photos can be done either using the rigorous digital photogrammetry or a polynomial transformation as used in the geometric correction (GC) module of the PCI system. The geometric correction was carried out in two steps: polynomial transformation and image resampling. All the scanned analog photos were geometrically corrected according to the digital orthophoto.

Step 3. Delineate land-cover types
A draft map was first sketched on the aerial photos (uncorrected) according to tones, structures, and patterns of defined land-cover types. This was used as reference for the final delineation of land-cover types on the digital version of airphotos. Using Imageworks of PCI we delineated cover types on the geometrically corrected aerial photos.

Step 4. Create the preliminary land-cover type map
With the MAP function in the PCI system, the result of delineation at step 3 were converted into a preliminary land-cover map. This map was exported into ARC/INFO and ARCVIEW systems for further processing.

Step 5. Finalize the land-cover map
With ARC/INFO and ARCVIEW, the preliminary land-cover type map was further processed by dividing or merging map units, generating area statistics and finalizing the map layout.

The Land-cover Prediction Model

Gray systems variable and process

In gray systems theory, an indeterminate variable is called a gray variable. Elements in a system with incomplete information are called gray elements. Define a gray element as $\otimes$ and its domain as $D(\otimes)$, then $\otimes \in D(\otimes)$. A gray variable is defined as $x(\otimes)$, $x(\otimes) = [a, b] \subset R$, R is a real number set. Given time t, and $t \in T$, then $x(\otimes, t)$ is a function of t, called a gray process. The gray process completely describes the behavior of a subject under study. $x^{(0)}_{(t)}$ contains complete information related to the subject of interest, including the part of determinate information, $x^{(0)}_{d(t)}$, and the part of indeterminate information, $x^{(0)}_{id(t)}$. Its expression is

$$x^{(0)}_{(t)} = x^{(0)}_{d(t)} + x^{(0)}_{id(t)} \qquad (1)$$

Accumulated generating operation, AGO

A time series $\{x^{(0)}_{(t)}\}, x^{(0)}_{(t)} \geq 0, t = 1, 2, ..., n$, may be calculated through AGO,

$$x^{(1)}_{(k)} = \sum_{t=1}^{k} x^{(0)}_{(t)} \qquad (2)$$

This generated time series $x^{(1)}_{(k)}$ is monotonically increasing. This may make some indeterminate gray variables increase their determination. Figure 1 dem-

onstrates this point with an example of population change of a county in China. The curve in Figure 1a clearly characterizes oscillation and stochasticality while the curve in Figure 1b is more stable and close to linear. AGO may also be based on the exponential law, called exponential AGO.

Inverse AGO is the inverse calculation of AGO. It may make the AGO series return to its original time series. In the construction of a prediction model, it is often used as increment information.

GM(1,1) model

A GST model with n orders and h variables is specified as *GM(n, h)*. The GMs with various n and h values can be used in different applications and require different data series. In this study, it is sufficient to only use a GM(1,1) model. A brief introduction to the GM(1,1) model is as following (Yuan, 1991).

GM(1,1) is one type of first-order differential equation as following:

$$\frac{dx}{dt} + ax = \mu \tag{3}$$

Equation (3) expresses a linear combination of a rate of change of variable x, $\frac{dx}{dt}$, with the variable itself, and the control variable μ. If an original data series $x^{(0)}_{(t)} = \{x^{(0)}_{(1)}, x^{(0)}_{(2)}, ..., x^{(0)}_{(n)}\}$

is calculated one time by AGO according to equation (2), then

$x^{(1)}_{(k)} = \{x^{(1)}_{(1)}, x^{(1)}_{(2)}, ..., x^{(1)}_{(n)}\}$

where, $t, k = 1, 2, ..., n$. The differential equation in the determinate form of the GM(1,1) model of $x^{(1)}_{(k)}$ is like

$$\frac{dx^{(1)}}{dt} + ax^{(1)} = \mu \tag{4}$$

where a and μ are parameters to be determined. After discretizing equation (4) and generating inverse AGO series, we have

$$x^{(0)}_{(k+1)} = a[-\frac{1}{2}(x^{(1)}_{(k)} + x^{(1)}_{(k+1)})] + \mu \tag{5}$$

$$\left.\begin{array}{l} x^{(0)}_{(2)} = a\left[-\frac{1}{2}(x^{(1)}_{(1)} + x^{(1)}_{(2)})\right] + \mu, \quad k = 1 \\ x^{(0)}_{(3)} = a\left[-\frac{1}{2}(x^{(1)}_{(2)} + x^{(1)}_{(3)})\right] + \mu, \quad k = 2 \\ \cdots\cdots\cdots\cdots\cdots\cdots\cdots\cdots \\ x^{(0)}_{(n)} = a\left[-\frac{1}{2}(x^{(1)}_{(n-1)} + x^{(1)}_{(n)})\right] + \mu, \quad k = n-1 \end{array}\right\} \tag{6}$$

If we define

$$Y_n = \begin{bmatrix} x^{(0)}_{(2)} \\ x^{(0)}_{(3)} \\ \vdots \\ x^{(0)}_{(n)} \end{bmatrix}, \tag{7}$$

$$\aleph = \begin{bmatrix} -\frac{1}{2}(x^{(1)}_{(1)} + x^{(1)}_{(2)}) \\ -\frac{1}{2}(x^{(1)}_{(2)} + x^{(1)}_{(3)}) \\ \cdots\cdots\cdots\cdots \\ -\frac{1}{2}(x^{(1)}_{(n-1)} + x^{(1)}_{(n)}) \end{bmatrix}, \text{ and}$$

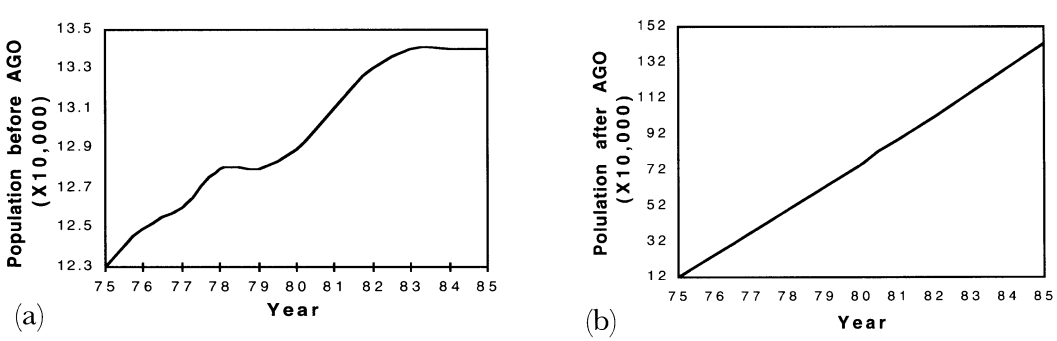

Figure 1. Population change across years before (a) and after (b) accumulated generating operation (modified from[15]).

$$E = \begin{bmatrix} 1 \\ 1 \\ \vdots \\ 1 \end{bmatrix}$$

then equation (6) can be rewritten as

$$Y_n = a\aleph + \mu E = [\aleph \vdots E]\begin{bmatrix} a \\ \mu \end{bmatrix} = [\aleph \vdots E]\hat{d} \qquad (8)$$

If we define

$$B = [\aleph \vdots E], \quad \hat{d} = [a, \mu]^T,$$

then

$$B = \begin{bmatrix} -\frac{1}{2}(x^{(1)}_{(1)} + x^{(1)}_{(2)}) & 1 \\ -\frac{1}{2}(x^{(1)}_{(2)} + x^{(1)}_{(3)}) & 1 \\ \cdots\cdots\cdots\cdots & 1 \\ -\frac{1}{2}(x^{(1)}_{(n-1)} + x^{(1)}_{(n)}) & 1 \end{bmatrix} \qquad (9)$$

Furthermore, equation (8) can be rewritten as

$$Y_n = B\hat{d} \qquad (10)$$

Where, parameter vector $\hat{d}$ can be obtained with the least squares method.

$$\hat{d} = (B^T B)^{-1} B^T Y_n \qquad (11)$$

Using $\hat{d} = [a, \mu]^T$ to replace equation (4) and solving the equation, we obtain

$$\hat{x}_{(t)} = \left(x^{(0)}_{(1)} - \frac{\mu}{a}\right)e^{-at} + \frac{\mu}{a}$$

When *t=t+1, x(t)=x(t+1),* for a one-time AGO data series $x^{(1)}_{(k)}$, then

$$\hat{x}^{(1)}_{(k+1)} = \left(x^{(0)}_{(1)} - \frac{\mu}{a}\right)e^{-ak} + \frac{\mu}{a} \qquad (12)$$

Therefore, the restored values of the AGO data series may be obtained from the following restored equation (13),

$$\begin{aligned} \hat{x}^{(0)}_{(k+1)} &= \hat{x}^{(1)}_{(k+1)} - \hat{x}^{(1)}_{(k)} \\ &= (1 - e^{a})\left(x^{(0)}_{(1)} - \frac{\mu}{a}\right)e^{-ak} \end{aligned} \qquad (13)$$

Equation (13) is a time-responding function of the GM(1,1) model. It is also a concrete realization of the GM(1,1) model for prediction.

The prediction procedure with the GM(1,1) model

The procedure of GST prediction with the GM(1,1) model can be divided into six steps:

step 1. Build an original data series,

$$x^{(0)}_{(t)} = \{x^{(0)}_{(1)}, x^{(0)}_{(2)}, \ldots, x^{(0)}_{(n)}\}$$

Step 2. Conduct a one-time AGO to $x^{(0)}_{(t)}$ with equation (2) to generate $x^{(1)}_{(k)}$,

$$x^{(1)}_{(k)} = \{x^{(1)}_{(1)}, x^{(1)}_{(2)}, \ldots, x^{(1)}_{(n)}\}$$

Step 3. With equations (7) and (9), construct matrices B and Yn.

Step 4. With equation (11), calculate

$$\hat{d} = [a, \mu]^T = (B^T B)^{-1} B^T Y_n$$

Step 5. With equation (13), obtain prediction values $\hat{x}^{(0)}_{(k)}$, $k = 2, 3, \ldots, n, n+1, \ldots$ $\hat{x}^{(0)}_{(n+1)}, \ldots$ are prediction values for the future.

Step 6. Analyze the prediction results.

If an original data series is not equal-interval of time, then it needs to be converted into an equal-interval time series before applying the GST prediction. The equal-interval of time series may be realized by linear interpolation, or using the method proposed by Yuan (1991). If the residual error of the prediction value is too big to be acceptable, the predicted values must be corrected by a residual error correction model. The residual error can be measured by the relative prediction error (RPE). RPE is defined as |V1-V2|/V1*100%, where V1, V2 are the actual and predicted values, respectively. The relative prediction accuracy (RPA) is defined as (1-RPE)*100%. If RPE > 15% then the model prediction is not acceptable. The correction model is similar to equation (13). The only difference is to use the residual errors of predicted values as the original data series and follow the six steps of GST prediction. A final prediction value (corrected) should be the prediction value by equation (13) plus or minus, depending on the sign of the residual error, the correction value obtained from the correction model.

IV. TEST AND RESULTS

Mapping Land-Cover Types

All five aerial photos were scanned into the PCI system. The digital orthophoto of 1995, which is relatively free from geometric distortion and contains more details than the other scanned images, was chosen as the master image to rectify the five other images. A total of 8 ground control points (GCPs) were collected for the image of 1947, 10 for the image of 1957, 11 for the image of 1969, and 12 for both images of 1979 and 1985. These GCPs were used to build second-order polynomials to register the five scanned images to the digital orthophoto. The regis-

tration results were quite satisfactory except for the image of 1947.

According to the definitions of the seven cover types (Table 1), a land-cover map was produced from each of the 6 dated aerial photos. The maps were input into ARC/INFO and ARCVIEW systems to be edited. Final land-cover type maps were generated (e.g., Figure 2. The percentage of land area for each cover type was calculated for each aerial photo. Figure 3 clearly shows the changes of the 7 land-cover types during the last five decades. From Figure 3, it can be seen that cover types RA and EU increased considerably in the past five decades while types BA and GL decreased. The other three types did not change much. It is not surprising to see the dramatic increase of RA because human development did not stop during this period (Sanders and Dow, 1993). According to the historical record, wildfire happened frequently in this area. Because Eucalyptus (EU) is a good burning fuel type, it is frequently burned. People liked and replanted the Eucalyptus because it grew faster than most other native species. Consequently, types RA and EU increased dramatically. These two types grew and invaded into type BA and GL causing the reduction of grassland and brush land during the last five decades. Although the other three types look unchanged, there still exist oscillations from the figure. This may be caused by delineation error or registration error or both. Figure 2 reflects the distribution of the 7 cover types at different dates. Basically, the land-cover maps indicate the change tendency of the land-cover types.

Prediction Results

Because the original data series is not of equal-time interval, we first interpolated the original data series into 10-year equal-intervals in time with the method proposed by Yuan (1991). The interpolated results (solid line) and the prediction results (dash line) obtained from the GM(1,1) model were illustrated in Figure 4. Both the interpolated and predicted values for each cover type at each time was normalized to sum up to 100% with all seven cover types. The prediction with GM(1,1) started from 1957 and ended at 2007 as a "real" prediction. From Figure 4, the interpolated results and the prediction results are

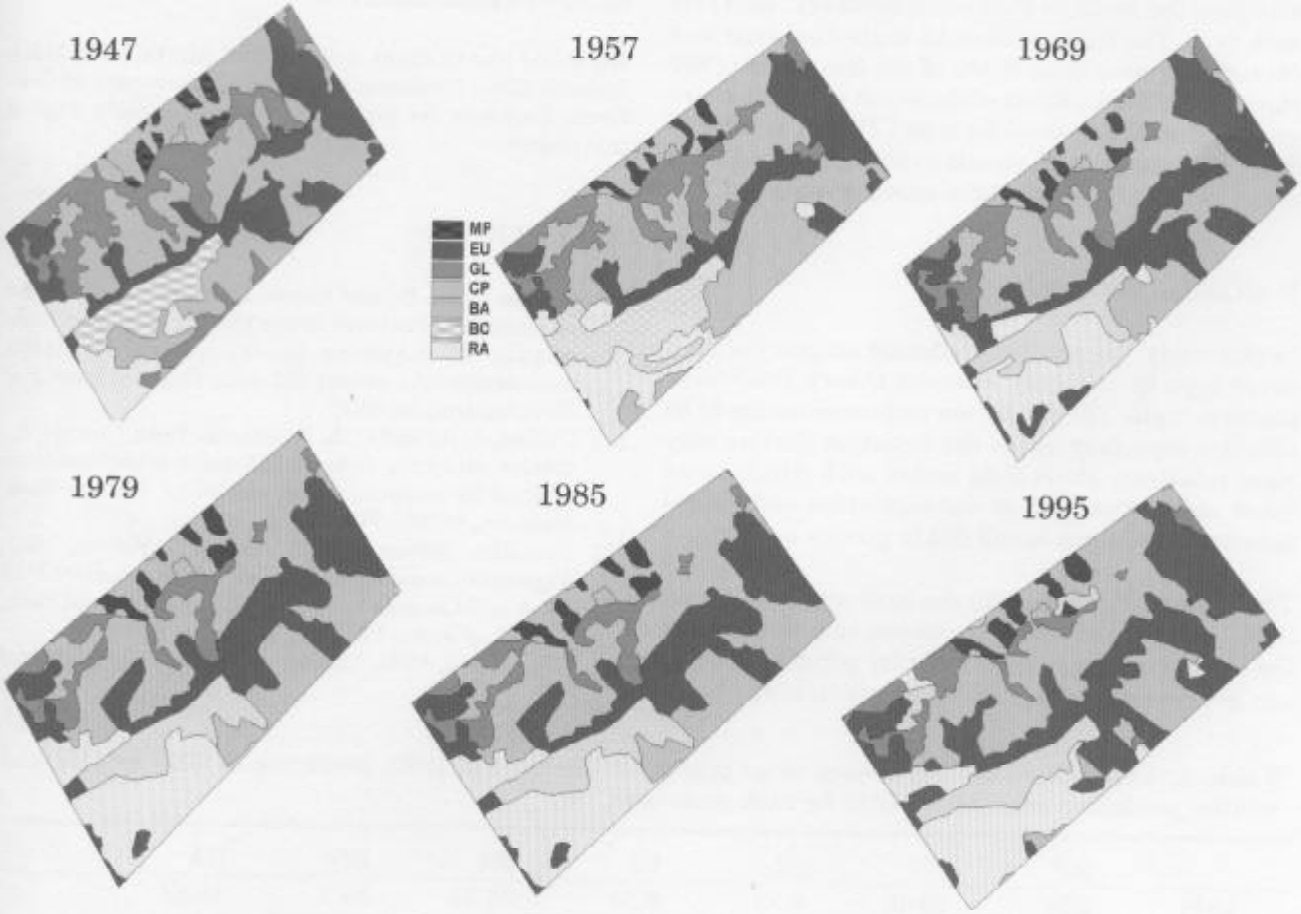

Figure 2. Land-cover types mapped from six dated aerial photos

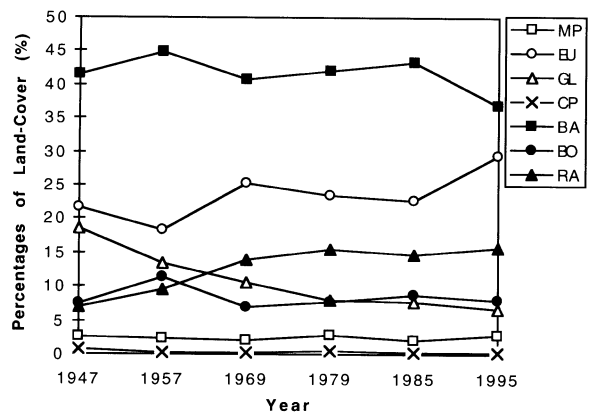

Figure 3. Percentage of land in each cover type delineated from six dated aerial photos

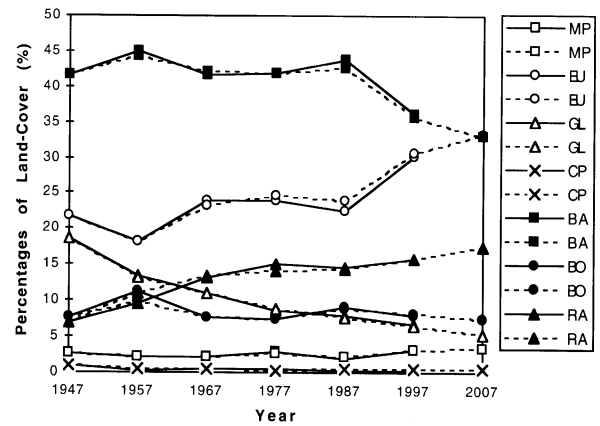

Figure 4. Percentage of land in each cover type for interpolated (solid line) from Figure 3 and predicted (dash line) by a GM model

quite consistent from 1957 to 1997. For the prediction result of 2007, the basic tendencies are extending the trends between 1987 and 1997. Table 2 lists the actual percentage of area for each cover type for 1995 and the prediction values for 2007. The table also lists the relative prediction accuracy (RPA) for each type. The RPA value of an individual type was obtained by averaging RPAs of the five times (1957 through 1997). All RPAs of the seven cover types are greater than 94% except for type CP with an RPA of 90%. The overall RPA equals to 95% generated from averaging the RPAs of all the seven cover types.

V. CONCLUSIONS

In this study, the relative prediction accuracy of each cover type by the gray systems theory prediction model is high. The prediction technique seems to be effective especially under the condition that we only have relatively short data series with which some other techniques such as the regression and neural network algorithms would fail to predict properly.

The prediction model with the gray systems theory (GST) built in this study, however, can only predict the cover percentage of a particular point in time. It can not predict the spatial distribution of the land-cover changes. A GST model that is capable of predicting the spatial distribution of land-cover changes is therefore desirable.

ACKNOWLEDGMENTS

We would like to thank John Radke, Mintai Kim, Mark Spencer, Dave Newburn, and Kirstin, University of California, Berkeley, for their helps during the early stage of this project.

REFERENCES

[1] Collins, John. B., and Curtis E. Woodcock, 1996, An assessment of several linear change detection techniques of mapping forest mortality using multitemporal Landsat TM data, *Remote Sensing of Environment*, 56:66-77.

[2] Collins, J. B., and C. E. Woodcock, 1994, Change detection using the Gramm-Schmidth transformation applied to mapping forest mortality, *Remote Sens. Environ.*, 50:267-279.

[3] Franklin, Steven E., and Bradley A. Wilson, 1991, Vegetation mapping and change detection using SPOT MLA and Landsat imagery in Kluane National Park, *Can. J. of R. S* ., 17(1):2-17.

[4] Gong, Peng, 1993, Change detection using principal

Table 2. Percentages of land in each cover type for delineation of 1995, prediction of 2007 by MG, and relative prediction accuracies (RPA) for each cover type. (%)

	MP	EU	GL	CP	BA	BO	RA
1995	2.96	29.48	6.79	0.34	36.77	8.03	15.67
2007	3.34	33.21	5.28	0.36	32.97	7.39	17.45
RPA	94.06	96.20	97.42	89.95	98.67	96.40	94.53

component analysis and fuzzy set theory, *Can. J. of R. S.*, 19(1):22-29.

[5] Gopal, Sucharita, and Curtis Woodcock, 1996, Remote sensing of forest change using artificial neural networks, *IEEE Transactions on Geoscience and Remote Sensing*, 34(2):398-404.

[6] Hashem, M. E., M. E. Nabil, and F. Haweta, 1996, Monitoring land cover of the desert fringes of the eastern Nile Delta, Egypt, *Proceeding of IGARSS'96*, Lincoln, Nebraska, pp. 1756-1758.

[7] Kauth, R. J., and G. S. Thomas, 1979, The tasseled cap—a graphic description of the spectral-temporal development of agricultural crops as seen by Landsat, in *Proceedings of the Symposium on Machine Processing of Remotely Sensed Data*, Purdue University, West Lafaette, IN, pp. 4b41-4b51.

[8] Kushwaha, S. P. S., 1990, Forest-type mapping and change detection from satellite imagery, *ISPRS J. of Photogrammetry and Remote Sensing*, 45:175-181.

[9] Miller, A. B., E. S. Bryant, and R. W. Birnie, 1998, An analysis of land cover changes in the Northern Forest of New England using multitemporal Landsat MSS data, *Int. J. Remote Sensing*, 19(2):245-265.

[10] Muchoney, Douglas M., and Barry N. Haack, 1994, Change detection for monitoring forest defoliation, *P. E. & R. S.*, 60(10):1243-1251.

[11] Parra, G. A., M. C. Mouchot, and C. Roux, 1996, A multitemporal land-cover change analysis tool using change vector and principal components analysis, *Proceeding of IGARSS'96*, Lincoln, Nebraska, pp. 1753-1755.

[12] PCI Inc., 1997, *EASI/PACE User's Manual (Version 6.2),* PCI Inc., Richmond Hill, Ontario, Canada.

[13] Sanders, Dale, and Steve Dow (editor), 1993, *Natural and cultural resource inventory of Claremont Canyon*, Final Report, University of California, Berkeley, p. 50.

[14] Tan, Sen S., and Fred E. Smeins, 1996, Predicting grassland community changes with an artificial neural network model, *Ecological Modelling*, 84:91-97.

[15] Yuan, J., 1991, *Gray System Theory and Its Application*, Science Press, Beijing, (In Chinese), pp.1-188.